

---

# Gas Dynamics in Clusters of Galaxies

C. L. Sarazin

Department of Astronomy, University of Virginia, P. O. Box 3818, Charlottesville, VA 22903-0818, USA  
sarazin@virginia.edu

## 1 Introduction

One of the more surprising results from X-ray astronomy is that the great volumes of space between galaxies in clusters of galaxies are not empty, as they appear in optical images. Instead, they are filled with a diffuse, hot plasma, with typical temperatures of  $T \sim 10^7\text{--}10^8$  K. At this temperature, the sound speed in the gas is comparable to the orbit velocities of the galaxies in the cluster, which is consistent with the gas being in hydrostatic equilibrium with the same gravitational potential as binds the galaxies. This intracluster medium (ICM) is highly rarefied, with electron number densities of  $n_e \sim 10^{-4}\text{--}10^{-2}$  cm $^{-3}$ . At least on large scales, the gas is stably stratified, with the density decreasing with increasing radius  $r$ . The gas extends out to distances of  $r \gtrsim$  Mpc from the cluster center. The total mass of hot gas is typically  $M_{\text{gas}} \sim 10^{14} M_{\odot}$ ; this mass exceeds the total mass of all the galaxies in a typical rich clusters, although even more of the mass is in the form of unseen “dark matter.”

At temperatures of  $10^6\text{--}10^8$  K, the dominant radiation mechanism of a plasma is X-ray emission. As a result, clusters of galaxies are generally very luminous X-ray emitters, with luminosities of  $L_X \sim 10^{43}\text{--}10^{45}$  ergs s $^{-1}$ . Clusters are second only to quasars as the most luminous X-ray sources in the Universe, and are the most luminous extended sources. While X-ray emission is the primary observational diagnostic for the intracluster medium, the ICM has a number of other important physical effects. It confines and distorts radio galaxies within the cluster. The cosmic ray and magnetic field components of the intracluster medium can also produce diffuse radio emission (see Feretti & Giovannini this volume). The ICM can strip interstellar gas from galaxies as they move through the cluster. Intracluster gas cools at the centers of many clusters, producing lower temperature gas. If the ICM contains dust, the dust will be strongly heated by the plasma, and may emit strongly in the infrared. The ICM also has a number of opacity effects; for example, it scatters and

heats the cosmic background radiation which passes through it. The magnetic field in the ICM leads to Faraday rotation and depolarization (Sect. 4.2).

In this chapter, I will review the physical state and X-ray emission processes of the ICM (Sect. 2 and 3). The ICM is shown to act as a fluid in Sect. 4. In Sect. 5, the transport properties of the gas, particularly thermal conduction, are discussed. The hydrodynamical equations for the ICM are given in Sect. 6. Models for the distribution of the gas, and the use of the gas to determine the total mass distributions of clusters are described in Sect. 7 and Sect. 8. The heating and cooling processes in the ICM are discussed in Sect. 9. Much of the heating is due to the hierarchical formation of clusters, and cluster mergers are introduced in Sect. 10. The thermal effects of merger shocks are discussed in Sect. 11. In Sect. 12, the effects of mergers on cluster cooling cores and the phenomena of cold fronts are described.

As much as possible, comparisons to observations in this chapter assume the standard WMAP cosmology [2], with a Hubble constant of  $H_0 = 71 \text{ km s}^{-1} \text{ Mpc}^{-1}$ , a ratio of the mass density to the critical density of  $\Omega_m = 0.27$ , and the ratio of the dark energy density to the critical density of  $\Omega_\Lambda = 0.73$ .

## 2 Physical State of the Intracluster Gas

### 2.1 Local Thermal State

At the very high temperatures of the intracluster gas, the gas is very highly ionized, but not completely so for the heavy elements. Thus, to describe the local thermal state of the gas, we need to specify three things. First, there are the motions of free particles (electrons and ions), or the kinetic state of the gas. Then, we need to give the ratios of electrons which are free to those which are bound to ions, or the ionization state of the gas. Finally, for the bound electrons, we need to which energy levels they occupy; this is the excitation state of the gas.

### Kinetic Equilibrium

If Coulomb collisions are sufficiently rapid, the free particles in the gas (free electron, free proton, and ions) will be brought into kinetic equilibrium and develop a Maxwellian distribution. The time scale for a particle of mass  $m_1$  and charge  $Z_1e$  to collide with field particles of mass  $m_2$  and charge  $Z_2e$  with a number density of  $n_2$  in a Maxwellian distribution at a temperature  $T$  is [43]:

$$t_{\text{eq}}(1, 2) = \frac{3m_1\sqrt{2\pi}(kT)^{3/2}}{8\pi\sqrt{m_2}n_2Z_1^2Z_2^2e^4 \ln \Lambda}. \quad (1)$$

Here,  $\ln \Lambda \equiv \ln(b_{\text{max}}/b_{\text{min}}) \approx 40$  is the Coulomb logarithm, and  $b_{\text{min}}$  and  $b_{\text{max}}$  are the minimum and maximum impact parameters for Coulomb collisions

in the gas. The Coulomb logarithm has a weak (logarithmic) dependence on density and temperature, but is nearly constant under ICM conditions. Coulomb collisions between electrons will bring the electrons into equilibration (an isotropic Maxwellian velocity distribution) on a time scale of roughly

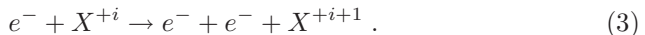
$$t_{\text{eq}}(e, e) \approx 3 \times 10^5 \text{ yr} \left( \frac{T}{10^8 \text{ K}} \right)^{3/2} \left( \frac{n_e}{10^{-3} \text{ cm}^{-3}} \right)^{-1} \text{ yr} . \quad (2)$$

The time scale for protons to equilibrate among themselves is  $t_{\text{eq}}(p, p) \approx (m_p/m_e)^{1/2} t_{\text{eq}}(e, e)$ , or roughly 43 times longer than the value in (2). Following this time, the protons and ions would each have Maxwellian distributions, but generally at different temperatures. The time scale for protons to collide with electrons and exchange energy is  $t_{\text{eq}}(p, e) \approx (m_p/m_e)t_{\text{eq}}(e, e)$ , or roughly 1870 times the value in (2). The time scale for the electrons and protons to come into equipartition (equal temperatures) is roughly one half of  $t_{\text{eq}}(p, e)$  [43].

Under typical conditions in the intracluster gas, these time scales are  $t_{\text{eq}}(e, e) \sim 10^5$  yr,  $t_{\text{eq}}(p, p) \sim 4 \times 10^6$  yr, and  $t_{\text{eq}}(p, e) \sim 2 \times 10^8$  yr. Most clusters have existed for  $\gtrsim 10^9$  yr, so one would expect the gas to generally be in kinetic equilibrium, with the distributions of free particles being isotropic Maxwellians. Moreover, the electrons and ions should generally be in equipartition, with a common kinetic temperature  $T = T_e = T_p$ . Possible exceptions might be the outermost regions of clusters (where the gas density is low), or regions where the gas properties have changed rapidly, such as shocks [26].

### Collisional Ionization Equilibrium

The main ionization process in the intracluster gas is collisional ionization,



The main recombination processes are radiative and dielectronic recombination,



Here,  $X^{+i}$  represents some element  $X$  which has been ionized  $i$  times. Note that neither radiative nor dielectronic recombination (4) are the inverse of collisional ionization (3), which implies that the ionization state in the intracluster gas is not that in thermodynamic equilibrium (the Saha equation).

Let  $C(X^i, T)$  be the rate coefficient for collisional ionization out of the ion  $X^i$  (3), while  $\alpha(X^i, T)$  is the rate coefficient for recombination to the ion  $X^i$  (4). If the gas starts in a lower ionization state than in equilibrium, it will be ionized up towards equilibrium on a time scale of roughly:

$$t_{\text{ion}} \approx [C(X^i, T)n_e]^{-1} \approx 3 \times 10^8 \left[ \frac{C(X^i, T)}{10^{-13} \text{ cm}^3 \text{ s}^{-1}} \right]^{-1} \left( \frac{n_e}{10^{-3} \text{ cm}^{-3}} \right)^{-1} \text{ yr} . \quad (5)$$

In general, the collisional ionization rates are high enough that one would expect the ICM to generally be in collisional ionization equilibrium. Again, possible exceptions might be the outermost regions of clusters (where the gas density is low), or regions where the gas properties have changed rapidly, such as shocks.

In collisional ionization equilibrium, the rates of collisional ionization and radiative and dielectronic recombination balance, which implies that

$$[C(X^i, T_g) + \alpha(X^{i-1}, T_g)] n(X^i) = C(X^{i-1}, T_g)n(X^{i-1}) + \alpha(X^i, T_g)n(X^{i+1}). \quad (6)$$

Here,  $n(X^i)$  is the number density of the  $X^i$  ion. Note that, unlike thermodynamic equilibrium (Saha equilibrium), the state of ionization in collisional ionization equilibrium is independent of density, and only depends on the electron kinetic temperature  $T$ . Generally, each ionization fraction reaches a maximum at a temperature that is some fraction of its ionization potential. At the temperatures which predominate in clusters, iron is mainly in the fully stripped, hydrogenic, or heliumlike stages.

### Excitation Equilibrium

For ions with bound electrons, the population of excited states are determined mainly by a balance between collision excitation by free electrons and radiative de-excitation. In general, the spontaneous radiative de-excitation rates are much higher than the excitation rates, and the electrons are almost always found in the ground level. The population of excited states are much lower than would be expected in thermodynamic equilibrium (Boltzmann distribution). Collisional de-excitation rates are much lower than radiative de-excitation rates; this means that there are no X-ray spectral diagnostics which determine the local density in the gas.

## 3 X-ray Emission

The X-ray emission of the intracluster gas is mainly due to thermal bremsstrahlung and line emission. There are smaller contributions of continuum from bound-free (recombination) emission and from two-photon decays of 2s levels in hydrogenic and helium-like ions.

The emissivity due to thermal bremsstrahlung (free-free emission) is given by

$$\epsilon_\nu^{\text{ff}} = \frac{2^5 \pi e^6}{3 m_e c^3} \left( \frac{2\pi}{3 m_e k} \right)^{1/2} n_e T^{-1/2} \exp(-h\nu/kT) \sum_i Z_i^2 n_i g_{\text{ff}}(Z_i, T, \nu), \quad (7)$$

where the emissivity  $\epsilon_\nu$  is defined as the emitted energy per unit time, frequency, and volume. The sum is over the various ions in the plasma, but is

dominated by hydrogen and helium for Solar abundances. The Gaunt factor  $g_{\#}(Z_i, T, \nu)$  corrects for quantum mechanical effects and for the effect of distant collisions, and is a slowly varying function of frequency and temperature. As a result, the dominant dependence of the free-free emissivity on frequency is the Boltzmann exponential factor, and the main dependences on temperature are this factor and the square-root factor  $T^{-1/2}$ . Thermal bremsstrahlung produces a roughly exponential continuum component in the X-ray spectrum. At high temperatures  $T \gtrsim 3 \times 10^7$  K, thermal bremsstrahlung is the dominant emission mechanism.

At lower temperatures, the main X-ray radiation is from lines. The strongest line feature observed from most clusters of galaxies is the complex of iron Fe K $\alpha$  lines at about 6.7 keV. This line feature is actually a blend of lines from iron ions (mainly Fe<sup>+24</sup> and Fe<sup>+25</sup>) and weaker lines from nickel ions. The notation ‘‘K $\alpha$ ’’ gives the principal quantum number  $n$  of the lower level of the transition and the change in the principal quantum number  $\Delta n \equiv n' - n$ , where  $n'$  is the principal quantum number of the upper level of the transition. K indicates that the lower level is in the K-shell ( $n = 1$ ), L indicates the lower level is in the L-shell ( $n = 2$ ), and so on, while  $\alpha$  indicates that  $\Delta n = 1$ ,  $\beta$  indicates that  $\Delta n = 2$ , etc. In addition to the Fe K line complex, the X-ray spectra of clusters of galaxies contain a large number of lower energy lines. These include the K lines of the common elements lighter than iron, such as C, N, O, Ne, Mg, Si, S, Ar, and Ca, as well as the L lines of Fe and Ni. These lines become very strong at lower temperatures ( $T \lesssim 10^7$  K).

As an illustration, Fig. 1 shows the predicted X-ray spectrum of an X-ray cluster [53]. The model cluster is isothermal in its outer regions (with a temperature of  $8 \times 10^7$  K), and has a cooling core at its center. The figure shows the overall exponential continuum from thermal bremsstrahlung, the Fe K lines at about 7 keV (which come mainly from the region of the cluster outside of the cooling flow), and the lower energy lines from the cooling core.

Most X-ray lines are excited by collisional excitation by electrons, although radiative and dielectronic recombination and inner shell collisional ionization also play a role. The emissivity due to a collisionally excited line is usually written [36]:

$$\int \epsilon_{\nu}^{\text{line}} d\nu = n(X^i)n_e \frac{h^3 \nu \Omega(T) B}{4\omega_{gs}(X^i)} \left[ \frac{2}{\pi^3 m_e^3 kT} \right]^{1/2} e^{-\Delta E/kT}, \quad (8)$$

where  $h\nu$  is the energy of the transition,  $\Delta E$  is the excitation energy above the ground state of the excited level,  $B$  is the branching ratio for the line (the probability that the upper state decays through this transition), and  $\Omega$  is the ‘collision strength’, which is often a slowly varying function of temperature.

The intracluster gas is almost certainly in collisional ionization equilibrium (Sect. 2.1); under these circumstances, the ionization fractions depend only on the electron temperature  $T$ , and are independent of the density of the gas. Then, the density of any ion is just proportional to the proton density in the

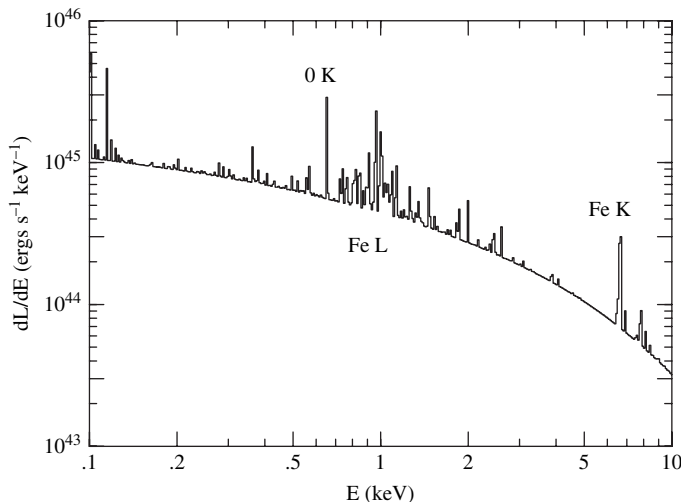


**Fig. 1.** Model X-ray spectrum of a cluster of galaxies. The cluster was assumed to be isothermal at  $T = 8 \times 10^7$  K in its outer regions, and to have a large amount of cool gas (a cooling core) in its inner regions

gas times the abundance of the relevant element relative to hydrogen. Thus, all of the X-ray emission processes in the gas scale with the product  $n_p n_e$  of the proton and electron densities, respectively. If  $L_\nu$  is the X-ray luminosity per unit frequency emitted by a cluster, then this can be written as

$$L_\nu = \Lambda_\nu(T, \text{Abundances}) \int n_e n_p dV, \quad (9)$$

where the integral is over the volume  $V$  of the cluster. The total emissivity  $\epsilon_\nu = \Lambda_\nu n_e n_p$ , where  $\Lambda_\nu$  depends only on the temperature and the abundances of the heavier elements relative to hydrogen. Similarly, the X-ray surface brightness is given by

$$I_\nu = \Lambda_\nu(T, \text{Abundances}) \int n_e n_p dl. \quad (10)$$

Here, the integral is along the line of sight distance  $l$  through the cluster.

The emissivity of a line is then proportional to the square of the density and to the abundance of the relevant element, and depends significantly on the electron temperature. Because the thermal bremsstrahlung emissivity also is proportional to the square of the density (7), the ratio of line emission to thermal bremsstrahlung continuum emission is independent of density. Line ratios or the shape of the X-ray continuum spectrum can be used to derive a temperature for the gas in a cluster. Then, the ratio of line emission to thermal bremsstrahlung continuum emission can be used to determine the abundance of the heavy element responsible for the line.

## 4 The Intracluster Medium as a Fluid

### 4.1 Mean Free Paths

The mean free paths of electrons and ions in a plasma without a magnetic field are determined by Coulomb collisions [43]. The electrons in a Maxwellian plasma undergo Coulomb collisions in a time which is a factor of  $\sqrt{m_e/m_p}$  shorter than the protons (Sect. 2.1). On the other hand, the electrons move faster by the inverse of this factor. Thus, the mean free paths of electrons and protons are essentially equal, with

$$\lambda_p = \lambda_e = \frac{3^{3/2}(kT)^2}{4\pi^{1/2}n_e e^4 \ln \Lambda} \approx 23 \left( \frac{T}{10^8 \text{ K}} \right)^2 \left( \frac{n_e}{10^{-3} \text{ cm}^{-3}} \right)^{-1} \text{ kpc}. \quad (11)$$

These mean free paths are smaller than most scales of interest in clusters; they are only about 1% of the radius of a cluster ( $\sim 2$  Mpc). Thus, it is reasonable to treat the ICM as a fluid under most circumstances. The fluid approximation might breakdown in the outer parts of a cluster (where the lower density increases  $\lambda_e$ ), in interactions with galaxies (whose sizes are comparable to  $\lambda_e$ ), if the ICM is very inhomogeneous, or in sharp transitions in the ICM properties at shocks or cold fronts (Sects. 11 and 12.2).

### 4.2 Magnetic Fields and Gyroradii

In any case, the ICM apparently contains a significant magnetic field, with typical values of  $B \sim 1 \mu\text{G}$ . (See the chapter by Feretti & Giovannini for more details concerning the magnetic field in clusters.) Stronger fields occur in some smaller volumes of clusters. These fields are probably too weak to be very important dynamically, as the magnetic pressure,  $P_B = B^2/(8\pi)$ , is much smaller than the typical gas pressures. However, the magnetic field does very strongly effect the microscopic motions of electrons and ions. In the presence of a magnetic field, electron and ions follow helical orbits, gyrating about magnetic field lines. The gyroradii of electrons and ions in cluster magnetic fields are very small. For example, the gyroradius of a typical electron is

$$r_g \approx 3 \times 10^8 \left( \frac{T}{10^8 \text{ K}} \right)^{1/2} \left( \frac{B}{1 \mu\text{G}} \right)^{-1} \text{ cm}. \quad (12)$$

These very small gyroradii probably insure that the ICM acts as a fluid even when the Coulomb mean free paths are long.

## 5 Transport Processes

The fact that the mean free paths are small but finite implies that the local properties of the gas will be influenced by the properties of the surrounding gas through diffusive processes, also called transport processes. These include

the thermal conduction of heat energy in non-isothermal gases, the viscous transport of momentum, and the diffusion and settling of heavy elements within the intracluster gas. I will concentrate on thermal conduction here; viscosity and diffusion are discussed in [40].

### 5.1 Thermal Conduction

In a plasma with a gradient in the electron temperature, heat is conducted down the temperature gradient. If the scale length of the temperature gradient  $l_T \equiv T/|\nabla T|$  is much longer than the mean free path of electrons,  $l_T \gg \lambda_e$ , then the heat flux is given by

$$\mathbf{Q} = -\kappa \nabla T, \quad (13)$$

where the thermal conductivity for a hydrogen plasma is [43]:

$$\begin{aligned} \kappa &= 1.31 n_e \lambda_e k \left( \frac{k T_e}{m_e} \right)^{1/2} \\ &\approx 4.6 \times 10^{13} \left( \frac{T_e}{10^8 \text{ K}} \right)^{5/2} \left( \frac{\ln \Lambda}{40} \right)^{-1} \text{ erg cm}^{-1} \text{ s}^{-1} \text{ K}^{-1}. \end{aligned} \quad (14)$$

Because of the inverse dependence on the particle mass, thermal conduction is primarily due to electrons. If the very weak dependence of  $\ln \Lambda$  on density is ignored, then  $\kappa$  is independent of density but depends very strongly on temperature.

If heat conduction operates at this ‘‘Spitzer’’ rate, then the gas in the central regions of clusters is likely to be isothermal. In addition, heat conduction would be very important at and would tend to eliminate any large local temperature gradients, such as appear to occur in the cooling core of clusters or near cold fronts (Sect. 12). On the other hand, the rate of thermal conduction along a thermal gradient perpendicular to the magnetic field is very low, as a result of the small gyroradii of electrons (12). Thus, transverse or tangled magnetic fields may be able to suppress thermal conduction in clusters, at least in some regions. The existence of very steep temperature gradients in cold fronts has been used to argue that heat conduction is suppressed by a factor of  $\gtrsim 10^2$  in these regions (Sect. 12.2).

## 6 Hydrodynamics

In the fluid limit, the ICM can be characterized by the local values of the gas density  $\rho$ , the gas pressure  $P$ , the gas temperature  $T$  or internal energy, and the gas velocity  $\mathbf{v}$ . The gas pressure is determined by the ideal gas law:

$$P = \frac{\rho k T}{\mu m_p}, \quad (15)$$

where  $\mu$  is the mean mass per particle in terms of the mass of a proton  $m_p$ . The dynamical equation for a single component fluid is [20]:

$$\rho \frac{D\mathbf{v}}{Dt} + \nabla P + \rho \nabla \Phi = 0, \quad (16)$$

where  $\Phi$  is the gravitational potential, and  $D/Dt$  is the Lagrangian derivative with respect to time. Equation (16) ignores non-gravitational forces, such as magnetic stresses or viscosity. The continuity equation (mass conservation) is [20]:

$$\frac{\partial \rho}{\partial t} + \nabla \cdot (\rho \mathbf{v}) = 0. \quad (17)$$

There is also an equation giving the variation in the energy in the fluid. However, it is simpler to give this equation in terms of the entropy in the gas,  $S$ . A useful quantity to consider is the specific entropy per particle in the gas,  $s \equiv S/N$ , where  $N$  is the total number of particles. To within additive constants, the specific entropy of an ideal gas is

$$s = \frac{3}{2} k \ln \left( \frac{P}{\rho^{5/3}} \right) = \frac{3}{2} k \ln \left( \frac{T}{\rho^{2/3}} \right). \quad (18)$$

To avoid the logarithmic character of the entropy, it is conventional to define an ‘‘entropy parameter’’  $K$  as

$$K \equiv \frac{kT}{(n_e)^{2/3}} \quad (19)$$

with units of keV cm<sup>2</sup>. Thus,  $s \propto \ln K$ . Then, the equation for the change in the gas entropy can be written [20]:

$$\frac{\rho}{\mu m_p} k \frac{Ds}{Dt} = \mathcal{H} - \mathcal{L}, \quad (20)$$

where  $\mathcal{H}$  and  $\mathcal{L}$  are the rate of heating and cooling per unit volume in the gas. In the absence of irreversible processes like heating or cooling or shocks, the specific entropy of a parcel of gas is constant.

## 7 Hydrostatic Equilibrium

Unless it is disturbed in some way, one would expect the gas in a cluster to relax into hydrostatic equilibrium on roughly the sound crossing time of the cluster,

$$t_s \equiv \frac{D}{c_s} \approx 6.6 \times 10^8 \text{ yr} \left( \frac{T}{10^8 \text{ K}} \right)^{-1/2} \left( \frac{D}{1 \text{ Mpc}} \right). \quad (21)$$

Here,  $D$  is the diameter of the cluster, and  $c_s$  is the sound speed. Since this time scale is shorter than the age of a typical cluster, which is a fraction

of the Hubble time, the gas in many clusters should be close to hydrostatic equilibrium. Exceptions would include clusters which are undergoing or have recently undergone a major merger, and regions of a cluster where an AGN has injected energy recently.

In hydrostatic equilibrium, the pressure forces balance gravity:

$$\nabla P = -\rho \nabla \Phi \quad , \quad \frac{1}{\rho} \frac{dP}{dr} = -\frac{GM(r)}{r^2} \quad , \quad (22)$$

where  $M(r)$  is the total cluster mass within  $r$ , and the second form assumes spherical symmetry. Because (22) gives a single relation for two gas properties (density and pressure), one must also specify the entropy distribution of the gas to determine its distribution.

### 7.1 Isothermal Models

A very simple model follows if the gas is assumed to be isothermal ( $T = \text{constant}$ ); isothermality might result if thermal conduction were efficient in the cluster (Sect. 5.1). Then, the solution of the hydrostatic equation is

$$\ln \left[ \frac{\rho(r)}{\rho_0} \right] = \frac{\mu m_p}{kT} [\Phi_0 - \Phi(r)] \quad , \quad (23)$$

where  $\rho_0$  and  $\Phi_0$  are the central values of the the gas density and gravitational potential, respectively. Note that the gas density will generally go to a finite value as  $r \rightarrow \infty$ .

Numerical simulations suggest that the dark matter distribution in clusters should have a power-law drop off at large radii, and a flatter power-law at small radii [35]. Thus, the dark matter distribution should have a cusp at the center of the cluster. The NFW dark matter profile [35] has:

$$\rho_{\text{DM}}(r) = \rho_s \left[ \left( \frac{r}{r_s} \right) \left( 1 + \frac{r}{r_s} \right)^2 \right]^{-1} \quad , \quad (24)$$

where  $r_s$  and  $\rho_s$  are the characteristic scaling radius and density, respectively. If this distribution applies to the sum of all the matter in a cluster, then the potential is

$$\Phi(r) = \Phi_0 \frac{\ln(1 + r/r_s)}{r/r_s} \quad , \quad (25)$$

and the central potential is  $\Phi_0 = -4\pi G \rho_s r_s^2$ .

However, in the past the dark matter and/or galaxy distributions in clusters were modeled using a function with a constant density core,

$$\rho_{\text{DM}}(r) = \rho_{\text{DM},0} \left[ 1 + \left( \frac{r}{r_c} \right)^2 \right]^{-3/2} \quad , \quad (26)$$

where  $\rho_{\text{DM},0}$  is the central density and  $r_c$  is the core radius. If this form is assumed for the total matter density in a cluster, or if it applies to the galaxy distribution, and the galaxies have an isotropic gaussian velocity distribution, then the resulting gas density distribution is the “beta model” [4]:

$$\rho(r) = \rho_o \left[ 1 + \left( \frac{r}{r_c} \right)^2 \right]^{-3\beta/2}. \quad (27)$$

If the gas is isothermal, then this density distribution gives an X-ray surface brightness distribution of the form

$$I_X(r) = I_X^o \left[ 1 + \left( \frac{r}{r_c} \right)^2 \right]^{-3\beta+1/2}. \quad (28)$$

This beta-model provides a reasonable fit to the X-ray surface brightness in the outer regions of many cluster, with a typical value of  $\beta \approx 2/3$ . However, it does not fit the inner parts of cooling core clusters.

## 7.2 Adiabatic or Polytropic Models

The temperature profiles in clusters of galaxies are generally more consistent with a gradual decline with radius at large radii, rather than isothermal gas [48]. A simple alternative would be if the gas in clusters was adiabatic (had a constant specific entropy); then the pressure and density would vary together as  $P \propto \rho^\gamma$  with  $\gamma = 5/3$ . Often, one also considers distributions with the same pressure-density relationship, but for values of  $\gamma$  in the range  $1 \leq \gamma \leq 5/3$ . We will refer to these distributions as “polytropic.” Then, the hydrostatic equation can be solved to give

$$\frac{T(r)}{T_0} = 1 + (\alpha - 1) \left[ 1 - \frac{\Phi(r)}{\Phi_0} \right], \quad (29)$$

$$\frac{\rho(r)}{\rho_0} = \left[ \frac{T(r)}{T_0} \right]^{1/(\gamma-1)}. \quad (30)$$

Here,  $T_0$  is the central temperature, and  $\alpha \equiv T(\infty)/T_0$ . The temperature profiles in the outer parts of clusters can generally be fit with intermediate values of  $\gamma \sim 1.2-1.3$  [24].

## 7.3 Surface Brightness Deprojection

The gas distributions in clusters can be derived directly from observations of the X-ray surface brightness of the cluster, if the shape of the cluster is known and if the X-ray observations are sufficiently detailed and accurate. The X-ray

surface brightness at a photon frequency  $\nu$  and at a projected distance  $b$  from the center of a spherical cluster is

$$I_\nu(b) = \int_{b^2}^{\infty} \frac{\epsilon_\nu(r) dr^2}{\sqrt{r^2 - b^2}}, \quad (31)$$

where  $\epsilon_\nu$  is the X-ray emissivity. This Abel integral can be inverted to give the emissivity as a function of radius,

$$\epsilon_\nu = -\frac{1}{2\pi r} \frac{d}{dr} \int_{r^2}^{\infty} \frac{I_\nu(b) db^2}{\sqrt{b^2 - r^2}}. \quad (32)$$

The emissivity  $\epsilon_\nu$  is proportional to the square of the density, and its spectral dependence is determined by the gas temperature and abundances (7), (8) and (9). Thus, the radial dependence of the spectrum and intensity of X-rays can be de-projected to the gas density  $\rho(r)$ , gas temperature  $T(r)$ , and abundances as a function of physical radius. The gas pressure is then given by the ideal gas law (15).

## 8 Cluster Masses

Once the gas density has been determined by either model fitting or de-projection, the gas mass can be derived simply as

$$M_{\text{gas}}(r) = 4\pi \int_0^r \rho(r') (r')^2 dr'. \quad (33)$$

Here,  $M_{\text{gas}}(r)$  is the gas mass interior to the radius  $r$ .

The total gravitational mass can be derived from the condition of hydrostatic equilibrium (22), which can be written as

$$M(r) = -\frac{r^2}{G\rho(r)} \frac{dP}{dr}, \quad (34)$$

where  $M(r)$  is the total mass interior to  $r$ . This equation can also be written as

$$M(r) = -\frac{kT(r)r}{\mu m_p G} \left[ \frac{d \ln \rho(r)}{d \ln r} + \frac{d \ln T(r)}{d \ln r} \right]. \quad (35)$$

Optical observations of the galaxies can be used to estimate the total mass of galaxies interior to  $r$ ,  $M_{\text{gal}}(r)$ . Any diffuse stellar light can be included in this; although these values can be difficult to determine, the stars and galaxies constitute only a small fraction of the mass, so this correction is not so important. Then, the mass of dark matter in the cluster (interior to  $r$ ) is given by

$$M_{\text{DM}}(r) = M(r) - M_{\text{gas}}(r) - M_{\text{gal}}(r) . \quad (36)$$

In typical clusters, the masses of stars and galaxies are much smaller than those of the hot gas, with  $M_{\text{gal}} \approx 0.15M_{\text{b}}$  at large radii [49]. Thus, hot plasma is the dominant form of baryonic matter in clusters of galaxies, with  $M_{\text{gas}} \approx 6M_{\text{gal}}$  at large radii. It appears that the same may be true on large scales throughout the present day Universe; it seems that most of the baryons in the Universe today are in hot, diffuse intergalactic gas (often called WHIM, or Warm Hot Intergalactic Medium), rather than stars and galaxies (e.g., [8]). In this sense, cluster represent the tip of the iceberg. With their very high densities, they are the one place it has been easy to detect the bulk of the baryons, which are in intergalactic gas.

The gas mass fraction  $f_{\text{gas}}(r)$  and baryon fraction  $f_{\text{b}}(r)$  are then

$$f_{\text{gas}}(r) = \frac{M_{\text{gas}}(r)}{M(r)} , \quad f_{\text{bary}}(r) = \frac{M_{\text{gas}}(r) + M_{\text{gal}}(r)}{M(r)} . \quad (37)$$

The observations of most clusters show an increase in  $f_{\text{gas}}(r)$  with radius  $r$  in the inner parts of clusters [1]. Thus, the gas is more broadly distributed than the dark matter in clusters. The gas fractions level out at radii which are  $r \gtrsim 0.2r_{\text{vir}}$ . Rich clusters have gas fractions which average  $\langle f_{\text{gas}}(r_{2500}) \rangle = 12\%$  at a radius where the mean interior density is 2500 times the critical density [1]. For typical clusters,  $r_{2500} \approx 0.25r_{\text{vir}}$ . The total gas fraction within  $r_{\text{vir}}$  will be a bit larger than this. Thus, clusters appear to consist of about 2–3% stars and galaxies, ~14% hot gas, and ~84% dark matter. Although these are recent values, clusters of galaxies provided some of the earliest evidence that the mass in the Universe was predominantly dark matter.

Clusters of galaxies are very useful cosmological probes. Arguably, they are the largest objects in the Universe which are dynamically relaxed. On the other hand, they are probably the smallest objects which formed from a sufficiently large volume that they contain a fair sample of the material in the Universe. Thus, the ratio of baryons to dark matter in clusters should be close to the universal value. Numerical simulations do indicate that the baryon fraction in clusters is nearly the general value in the Universe; even at  $r_{2500}$ ,  $f_{\text{bary}}$  is about 82% of the universal value [10].

When combined with the density of baryons inferred from Big Bang nucleosynthesis, the observed baryon fraction in clusters indicates that the total mass density in the Universe is  $\Omega_m \approx 0.3$  [52]. Thus, cluster have provided some of the earliest and strongest evidence that we live in a low density Universe, with too little matter to close the Universe and reverse the expansion of the Big Bang.

The measured values of  $f_{\text{gas}}$  and  $f_{\text{bary}}$  depend on the distance  $d$  to a cluster as  $d^{3/2}$ . On the other hand, if clusters are fair samples of the materials in the Universe, then  $f_{\text{bary}}$  should be independent of redshift or distance. Thus, a comparison of  $f_{\text{bary}}$  in low redshift and high redshift clusters provides a measure of the distance to the clusters which is independent of the redshift.

Such measurements provide evidence that we live in an accelerating Universe, with an effective cosmological constant of  $\Omega_\Lambda \approx 0.7$  [1]. This is in concordance with the results from WMAP [2] and supernova Type Ia observations at high redshifts.

## 9 Heating and Cooling of Intracluster Gas

### 9.1 Why Is the ICM So Hot?

When it was first observed in X-rays, one of the most surprising features about the intracluster gas was its very high temperature. Why is this gas so hot? In fact, this is one of the easiest aspects of the ICM to understand. At least in rich clusters, most of the heating is gravitational in origin. The basic idea is that clusters have huge masses, and very deep gravitational potential wells. Essentially, any means of introducing the gas into a cluster will cause it to move very rapidly, and collide with other gas, and be shocked. For example, if the gas fell into the cluster (either at the same time as the dark matter, or subsequently), cluster gravitational potentials imply that the gas would fall in at a speed  $\gtrsim 1000 \text{ km s}^{-1}$ . Unless the gas motions were very carefully controlled, the gas would encounter other gas moving at similar velocities, and the intersecting gas streams would collide and shock. Since the ICM has heavy elements, a portion of it came out of galaxies. If it did so after the clusters formed, then the galaxies would be moving at orbital speeds of  $\gtrsim 1000 \text{ km s}^{-1}$  in the cluster, and gas ejected from different galaxies would collide and shock at these sorts of speeds. (If the gas came out of galaxies before clusters formed, then it had to fall into a cluster, and was shocked as described previously.) Thus, it is likely that essentially all of the gas in the ICM medium shocked at speeds of  $\gtrsim 1000 \text{ km s}^{-1}$ , and was heated in this way.

In actually, we believe that clusters form hierarchically from the merger of smaller groups and clusters. Such mergers are discussed extensively below (Sect. 10). Thus, the specific mechanism for much of the heating of the ICM is likely to be merger shocks.

### 9.2 Simple Scaling Laws for Gravitational Heating

If one assumes that gravitational heating dominates in clusters, and makes a few other simple assumptions, it is possible to derive a number of simple scaling laws for the X-ray properties of clusters [18]. If the gas in clusters is in hydrostatic equilibrium and is distributed similarly to the dark matter, then the typical gas temperature should be  $kT \sim \mu m_p GM/R$ , where  $M$  is the total cluster mass, and  $R$  is the cluster radius. If one can treat the formation of a cluster as equivalent to the collapse of a isolated, spherical region of overdensity in the Universe, then the post-collapse average density in the

cluster should be  $\langle \rho_{\text{tot}} \rangle \sim 180 \rho_{\text{crit}}(z_{\text{form}})$ , where  $\rho_{\text{tot}}$  is the total mass density (dark matter and baryons), and  $\rho_{\text{crit}}(z_{\text{form}})$  is the critical density for the Universe to collapse at the epoch of formation of the cluster. If most clusters have formed recently, then one could approximate  $z_{\text{form}} \sim 0$ . Finally, clusters are large enough to contain a fair sample of the material in the Universe, and thus it is reasonable to assume that the baryon fraction in clusters (which is predominantly in the hot gas) is the universal value (Sect. 8). Then, the radii of clusters should scale with mass as

$$R \propto M^{1/3} . \quad (38)$$

The gas temperature would scale as

$$T \propto M^{2/3} , \quad (39)$$

and the X-ray luminosity vs. temperature relationship would be

$$L_X \propto T^2 . \quad (40)$$

The latter scaling assumes that the X-ray emission is mainly due to thermal bremsstrahlung, which is true for hot clusters.

### 9.3 Non-Gravitational Heating

There are a number of indications that non-gravitational heating or cooling processes may affect the ICM, particularly in smaller clusters and groups. First, the observed cluster X-ray properties do not agree very well with the scaling relations for purely gravitational heating (38), (39) and (40). Probably, the most significant deviation is that the measured X-ray luminosity–temperature relation is much steeper than (40) [23]. The departures for the scaling relations are particularly strong for cooler clusters and groups. Second, the observed gas distributions in clusters are more extended than would be expected from purely gravitational heating. The gas distributions often have central cores. This suggests that some non-gravitational heating processes have occurred and have puffed up the gas distributions, particularly in the poorer clusters. This would lower the average density in the gas, and thus reduce the X-ray luminosity. An alternative possibility is that inhomogeneous cooling has removed the cooler ICM, increasing the average temperature of the gas which remains. Presumably, this cooling would also lead to star and galaxy formation. These topics have been reviewed extensively in [50].

If the non-gravitational heating occurred just prior to the collapse of a cluster, then the amount of heat needed is  $\sim 2$  keV per particle [21]. However, a more useful quantity to describe the preheating is probably the extra entropy per particle  $\Delta s$  (18). As noted in Sect. 6, the specific entropy is a Lagrangian quantity which moves with the gas, and which remains constant for reversible changes. As discussed in Sect. 6, it is conventional to use the

entropy parameter  $K$  (19) rather than  $s$ . For purely gravitational heating, the scaling laws described above (Sect. 9.2) imply that the entropy parameter is expected to scale as

$$K \propto T \propto M^{2/3}. \quad (41)$$

Observations of clusters and groups initially suggested that preheating produced an extra entropy of  $\Delta K \approx 135 \text{ keV cm}^{-2}$  [22, 37]. It now appears that such an “entropy floor” may be too simplified to explain the detailed variations in entropy between clusters and the radial variations within clusters. Also, the existence of the Lyman alpha forest and other quasar absorption lines indicates that not all of the intergalactic gas underwent the same level of preheating. Nonetheless, this value provides a useful value in assessing models for the thermal history of the ICM.

The radial variation of the entropy in the ICM also appears to be inconsistent with purely gravitational heating. Gravitational heating models predict that the entropy vary roughly as  $K \propto r^{1.1}$ . The observed entropy profiles in clusters are much flatter in the center [38].

Supernovae could provide a significant source of heating of the ICM. These would include core collapse supernova associated with the deaths of massive stars. Since the galaxies in clusters today contain very few such stars, this would have occurred during the epoch of star formation and galaxy formation. The supernovae might have driven galactic winds. The second type of supernovae are Type Ia’s, which are produced by older binary star systems. They would provide a more continuous source of heating.

Supernovae also eject heavy elements. Thus, the abundances in clusters can be used to limit the total number of supernova which have occurred. The observed abundances suggest that the extra energy added is probably  $\sim 0.3$  keV per particle [21]. This is a bit low to explain the required preheating, but might be possible. However, this mechanism would also require that a large fraction of the supernova explosion energy be converted into heat in the ICM, which may also be a difficulty.

Active galactic nuclei (AGNs) within clusters might also provide a significant amount of heating. As with the supernovae, it is difficult to determine what fraction of the energy produced by AGNs goes into heating the surrounding medium. In this regard, it is only the AGN output in kinetic energy in jets or in relativistic particles which is likely to be useful. It may be important that the early-type galaxies found in clusters generally host radio galaxies and radio quasars, which are more likely to deposit energy into the ICM.

One way to limit the total energy input by AGNs is to look at the total masses of supermassive black holes contained in clusters today. In general, all large bulges appear to contain supermassive black holes, and there is a strong correlation of black hole mass with bulge mass or velocity dispersion. If the growth of black holes occurred largely by accretion (rather than merging of existing massive black holes), then the total accretion energy from black holes

can be derived from their total mass. This could provide a significant level of heating for the ICM if the fraction of accreted energy which goes into heating is  $\gtrsim 10\%$  [5].

#### 9.4 Cooling in the Intracluster Medium

The primary cooling process for the ICM is the emission of X-ray radiation. The emission is proportional to the square of the density and varies with temperature (7), (8), and (9). Thus, the total cooling rate per unit volume  $\mathcal{L}$  in the gas can

$$\mathcal{L} = \Lambda(T, \text{Abundances}) n_e n_p, \quad (42)$$

where  $\Lambda$  depends only on the temperature and the abundances of the heavier elements relative to hydrogen. At high temperature ( $kT \gtrsim 2$  keV), the dominant radiation is thermal bremsstrahlung, and  $\Lambda \propto T^{1/2}$ . At lower temperature, line emission becomes dominant, and  $\Lambda$  decreases with increasing temperature.

At high temperatures where thermal bremsstrahlung dominates, the time required for gas to cool to low temperatures at constant pressure is

$$t_{\text{cool}} = 69 \left( \frac{n_e}{10^{-3} \text{ cm}^{-3}} \right)^{-1} \left( \frac{T}{10^8 \text{ K}} \right)^{1/2} \text{ Gyr}. \quad (43)$$

Note that cooling accelerates as the gas cools; this tendency is even stronger below  $kT \lesssim 2$  keV due to line emission. The cooling time is much longer than the Hubble time in the outer parts of clusters. However, it can be quite short ( $t_{\text{cool}} \sim 300$  Myr) in the inner regions of cooling core clusters.

It is interesting to write the cooling time as a function of the entropy and temperature rather than the density and temperature:

$$t_{\text{cool}} = 17 \left( \frac{K}{130 \text{ keV cm}^{-2}} \right)^{3/2} \left( \frac{kT}{2 \text{ keV}} \right)^{-1} \text{ Gyr}. \quad (44)$$

Note that the cooling time is less than the Hubble time for  $K \lesssim 130 \text{ keV cm}^{-2}$  for  $kT \sim 2.5$  keV. If clusters start with gas with a wide range of entropies, the lower entropy gas will cool rapidly and be removed from the ICM. Thus, cooling can increase the average entropy of the gas and provide an effective “floor” to the ICM entropy [51]. The cooled gas presumably goes into forming galaxies and stars. Feedback heating from supernovae, galactic winds, and AGNs (Sect. 9.3) might result in some of the cooled gas actually becoming hotter ICM. However, the result is to remove the cooler gas and raise the average entropy of the ICM.

Thus, while the bulk of the heating of the ICM in large clusters is due to gravitational heating, mainly by merger shocks, smaller clusters and the centers of clusters show evidence for the effects of non-gravitational heating and cooling. The cooling leads to star and galaxy formation, and which leads

to possible heating by supernovae, galactic winds, and AGNs. Thus, the ICM (and intergalactic medium more generally) preserve a unique record of the thermal history of the Universe.

## 10 Cluster Mergers

Major cluster mergers are the most energetic events in the Universe since the Big Bang. Cluster mergers are the mechanism by which clusters are assembled. In these mergers, the subclusters collide at velocities of  $\sim 2000$  km/s, releasing gravitational binding energies of as much as  $\gtrsim 10^{64}$  ergs. During mergers, shocks are driven into the intracluster medium. In major mergers, these hydrodynamical shocks dissipate energies of  $\sim 3 \times 10^{63}$  ergs; such shocks are the major heating source for the X-ray emitting intracluster medium. The shock velocities in merger shocks are similar to those in supernova remnants in our Galaxy, and we expect them to produce similar effects. Mergers shocks should heat and compress the X-ray emitting intracluster gas, and increase its entropy. We also expect that particle acceleration by these shocks will produce relativistic electrons and ions, and these can produce synchrotron radio, inverse Compton (IC) EUV and hard X-ray, and gamma-ray emission. (See the chapter by Feretti & Giovannini for more details relativistic particles and non-thermal emission in clusters.)

## 11 Thermal Physics of Merger Shocks

The intracluster medium (ICM) is generally close to hydrostatic equilibrium in clusters which are not undergoing strong mergers. The virial theorem then implies that the square of the thermal velocity (sound speed) of the ICM is comparable to the gravitational potential. During a merger, the infall velocities of the subclusters are comparable to the escape velocity, which implies that the square of the infall velocity is larger (by roughly a factor of two) than the gravitational potential. Thus, the motions in cluster mergers are expected to be supersonic, but only moderately so. As a result, one expects that cluster mergers will drive shock waves into the intracluster gas of the two subclusters. Let  $v_s$  be the velocity of such a shock wave relative to the preshock intracluster gas. The sound speed in the preshock gas is  $c_s = \sqrt{(5/3)P/\rho}$ , where  $P$  is the gas pressure and  $\rho$  is the density. Then, the Mach number of the shock is  $\mathcal{M} \equiv v_s/c_s$ . Based on the simple argument given above, one expects shocks with Mach numbers of  $\mathcal{M} \lesssim 2$ . Stronger shocks may occur under some circumstances, such as in the outer parts of clusters, or in low mass subclusters merging with more massive clusters.

Shocks are irreversible changes to the gas in clusters, and thus increase the entropy  $S$  in the gas. A useful quantity to consider is the specific entropy per particle in the gas,  $s$  (18). Observations of X-ray spectra can be used to

determine  $T$ , while the X-ray surface brightness depends on  $\rho^2$ . Thus, one can use X-ray observations to determine the specific entropy in the gas just before and just after apparent merger shocks seen in the X-ray images. Since merger shocks should produce compression, heating, pressure increases, and entropy increases, the corresponding increase in all of these quantities (particularly the entropy) can be used to check that discontinuities are really shocks (e.g., not “cold fronts” or other contact discontinuities, Sect. 12.2).

In [26], this test was applied to ASCA temperature maps and ROSAT images of Cygnus-A and Abell 3667, two clusters which appeared to show strong merger shocks. Recent Chandra images have shown that the feature in Abell 3667 is a cold front [47]. In Cygnus-A, the increase in specific entropy in the shocked regions is roughly  $\Delta s \approx (3/2)k$ . The specific heat per particle  $q$  which must be dissipated to produce this change in entropy is  $q \approx T\Delta s \approx (3/2)kT$ , or about the present specific heat content in the shocked gas. Thus, these observations provide a direct confirmation that merger shocks contribute significantly to the heating of the intracluster gas.

The most dramatic merger shock which has been seen with Chandra is in the “Bullet Cluster” 1E0657-56 [7, 29, 30]. This is a very high velocity ( $\sim 4500$  km s $^{-1}$ ) merger occurring nearly in the plane of the sky, with a merger bow shock located ahead of a “cold front” (Sect. 12.2). Another prominent merger shocks with a Mach number of  $\mathcal{M} \approx 2.1$  is seen in Abell 520 [25]. In both cases, the merger shocks appear to have associated diffuse radio emission (See the chapter by Feretti & Giovannini for more details.)

### 11.1 Shock Kinematics

The variation in the hydrodynamical variables in the intracluster medium across a merger shock are determined by the standard Rankine–Hugoniot jump conditions [20], if one assumes that all of the dissipated shock energy is thermalized. Consider a small element of the surface of a shock (much smaller than the radius of curvature of the shock, for example). The tangential component of the velocity is continuous at the shock, so it is useful to go to a frame which is moving with that element of the shock surface, and which has a tangential velocity which is equal to that of the gas on either side of the shock. In this frame, the element of the shock surface is stationary, and the gas has no tangential motion. Let the subscripts 1 and 2 denote the preshock and post-shock gas; thus,  $v_1 = v_s$  is the longitudinal velocity of material into the shock (or alternative, the speed with which the shock is advancing into the preshock gas). Conservation of mass, momentum, and energy then implies the following jump conditions

$$\begin{aligned} \rho_1 v_1 &= \rho_2 v_2, \\ P_1 + \rho_1 v_1^2 &= P_2 + \rho_2 v_2^2, \\ w_1 + \frac{1}{2} v_1^2 &= w_2 + \frac{1}{2} v_2^2. \end{aligned} \tag{45}$$

Here,  $w = P/\rho + \epsilon$  is the enthalpy per unit mass in the gas, and  $\epsilon$  is the internal energy per unit mass. If the gas behaves as a perfect fluid on each side of the shock, the internal energy per unit mass is given by:  $\epsilon = /(\gamma - 1) P/\rho$ , where  $\gamma$  is the ratio of specific heats (the adiabatic index) and is  $\gamma = 5/3$  for fully ionized plasma. The jump conditions can be rewritten as:

$$\frac{P_2}{P_1} = \frac{2\gamma}{\gamma + 1} \mathcal{M}^2 - \frac{\gamma - 1}{\gamma + 1}$$

$$\frac{v_2}{v_1} = \frac{\rho_1}{\rho_2} \equiv \frac{1}{C} = \frac{2}{\gamma + 1} \frac{1}{\mathcal{M}^2} + \frac{\gamma - 1}{\gamma + 1}, \quad (46)$$

where  $C \equiv \rho_2/\rho_1$  is the shock compression.

If one knew the velocity structure of the gas in a merging cluster, one could use these jump condition to derive the temperature, pressure, and density jumps in the gas. At present, the best X-ray spectra for extended regions in clusters of galaxies have come from CCD detectors on ASCA, Chandra, and XMM/Newton. CCDs have a spectral resolution of  $>100$  eV at the Fe K line at 7 keV, which translates into a velocity resolution of  $>4000$  km/s. Thus, this resolution is (at best) marginally insufficient to measure merger gas velocities in clusters. In a few cases with very bright regions and simple geometries, the grating spectrometers on Chandra and especially XMM/Newton may be useful.

At present, X-ray observations can be used to directly measure the temperature and density jumps in merger shocks. Thus, one needs to invert the jump relations to give the merger shock velocities for a given shock temperature, pressure, and/or density increase. If the temperatures on either side of the merger shock can be measured from X-ray spectra, the shock velocity can be inferred from [26]:

$$\Delta v_s = \left[ \frac{kT_1}{\mu m_p} (C - 1) \left( \frac{T_2}{T_1} - \frac{1}{C} \right) \right]^{1/2}, \quad (47)$$

where  $\Delta v_s = v_1 - v_2 = [(C - 1)/C]v_s$  is the velocity change across the shock, and  $\mu$  is the mean mass per particle in units of the proton mass  $m_p$ . The shock compression  $C$  can be derived from the temperatures as

$$\frac{1}{C} = \left[ \frac{1}{4} \left( \frac{\gamma + 1}{\gamma - 1} \right)^2 \left( \frac{T_2}{T_1} - 1 \right)^2 + \frac{T_2}{T_1} \right]^{1/2} - \frac{1}{2} \frac{\gamma + 1}{\gamma - 1} \left( \frac{T_2}{T_1} - 1 \right). \quad (48)$$

Alternatively, the shock compression can be measured directly from the X-ray image. However, it is difficult to use measurements of the shock compression alone to determine the shock velocity, for two reasons. First, a temperature is needed to set the overall scale of the velocities; as is obvious from (46), the shock compression allows one to determine the Mach number  $\mathcal{M}$  but not the shock velocity. The second problem is that temperature or pressure

information is needed to know that a discontinuity in the gas density is a shock, and not a contact interface (e.g., the “cold fronts” discussed in Sect. 12.2 below).

X-ray temperature maps of clusters have been used to derive the merger velocities using these relations. Reference [26] used ASCA observations to determine the kinematics of mergers in three clusters (Cygnus-A, Abell 2065, and Abell 3667). Because of the poor angular resolution of ASCA, these analyses were quite uncertain. More recently, possible shocks have been detected in Chandra images of a number of merging clusters (e.g., Abell 85 [19], Abell 665 [27], Abell 3667 [47]), and the shock jump conditions have been applied to determine the kinematics in these clusters.

The simplest case is a head-on symmetric merger ( $b = 0$  and  $M_1 = M_2$ ) at an early stage when the shocked region lies between the two cluster centers. Reference [26] suggests that the Cygnus-A cluster is an example. If the gas within the shocked region is nearly stationary, then the merger velocity of the two subclusters is just  $v = 2\Delta v_s$ . Applying these techniques to the ASCA temperature map for the Cygnus-A cluster, Reference [26] found a merger velocity of  $v \approx 2200$  km/s. This simple argument is in reasonable agreement with the results of numerical simulations of this merger [39].

One can compare the merger velocities derived from the temperature jumps in the merger shocks with the values predicted by free-fall from the turn-around radius. In the case of Cygnus-A, [26] found good agreement with the the free-fall velocity of  $\sim 2200$  km/s. This consistency suggests that the shock energy is effectively thermalized, and that a major fraction does not go into turbulence, magnetic fields, or cosmic rays. Thus, the temperature jumps in merger shocks can provide an important test of the relative roles of thermal and non-thermal processes in clusters of galaxies.

## 11.2 Nonequilibrium Effects

Cluster mergers are expected to produce collisionless shocks, as occurs in supernova remnants. As such, nonequilibrium effects are expected, including non-equipartition of electrons and ions and nonequilibrium ionization [26, 44, 45]. Collisionless shocks are generally not as effective in heating electrons as ions. Assuming that the post-shock electrons are somewhat cooler than the ions, the time scale for electron and protons to approach equipartition as a result of Coulomb collisions in a hot ionized gas is (2) [43]:

$$\begin{aligned}
 t_{\text{eq}} &= \frac{3m_p m_e}{8\sqrt{2\pi} n_e e^4 \ln \Lambda} \left( \frac{kT_e}{m_e} \right)^{3/2} \\
 &\approx 2.1 \times 10^8 \left( \frac{T_e}{10^8 \text{ K}} \right)^{3/2} \left( \frac{n_e}{0.001 \text{ cm}^{-3}} \right)^{-1} \text{ yr}, \quad (49)
 \end{aligned}$$

where  $n_e$  and  $T_e$  are the electron number density and temperature, respectively, and  $\Lambda$  is the Coulomb factor. The relative velocity between the

post-shock gas and the shock front is  $(1/4)v_s$ ; thus, one would expect the electron temperature to reach equipartition a distance of

$$d_{\text{eq}} \approx 160 \left( \frac{v_s}{3000 \text{ km/s}} \right) \left( \frac{T_e}{10^8 \text{ K}} \right)^{3/2} \left( \frac{n_e}{0.001 \text{ cm}^{-3}} \right)^{-1} \text{ kpc} \quad (50)$$

behind the shock front. Of course, it is the electron temperature (rather than the ion or average temperature) which determines the shape of the X-ray spectrum. This distance is large enough to insure that the lag could be spatially resolved in X-ray observations of low redshift clusters. Similar effects might be expected through non-equilibrium ionization.

On the other hand, it is likely that the nonequilibrium effects in cluster merger shocks are much smaller than those in supernova blast wave shocks because of the low Mach numbers of merger shocks. That is, the preshock gas is already quite hot (both electrons and ions) and highly ionized. Moreover, a significant part of the heating in low Mach number shocks is due to adiabatic compression, and this would still act on the electrons in the post-shock gas in merger shocks, even if there were no collisionless heating of electrons. For example, in a  $\mathcal{M} = 2$ ,  $\gamma = 5/3$  shock, the total shock increase in temperature is a factor of 2.08 (46). The shock compression is  $C = 2.29$ , so adiabatic compression increases the electron temperature by a factor of  $C^{2/3} = 1.74$ , which is about 83% of the shock heating.

### 11.3 Mergers and Basic Gravitational Physics Effects

Merging clusters also provide several very direct tests of basic gravitational physics. These tests are possible because of the dynamical nature of mergers, and the difference in the behavior of collisional and non-collisional components of clusters. The gas in clusters is a collisional fluid (Sect. 4) with a mean-free-path which is small compared to the scale of clusters (11). Thus, when clusters collide, the motion of the gas will be retarded by ram pressure and shocks. On the other hand, the galaxies in clusters are essentially collisionless. When clusters collide, the galaxies will fly by one another. Thus, the galaxies in a merging subcluster will often be found ahead of the gas from the same subcluster. This is particularly obvious in late stage mergers with “cold fronts” (Sect. 12.2), where the gas which was initially at the center of a subcluster will be found lagging behind the central dominant and other galaxies from the subcluster. Perhaps the most prominent example of this is the in the “Bullet Cluster” 1E0657-56 [7, 29, 30], where the cold front and dense gas from the subcluster are clearly separated for the galaxies from the same subcluster.

In the most widely accepted model for “dark matter” (Sect. 8), the dominant component of the mass of the Universe is made up of collisionless elementary particles. For example, this would be true of Cold Dark Matter (e.g., [2]). If this is the case, one would expect that the dark matter would be located in the same regions of merging clusters as the galaxies. An alternative

idea is that the law of gravity or laws of motions differ from the Newtonian form at large distances or small accelerations [33]. In these MODified Newtonian Dynamics (MOND) theories, there is no dark matter component of the Universe, and gravity is just due to ordinary baryonic matter. In clusters of galaxies, the vast majority of the ordinary baryonic matter is in the hot X-ray gas (Sect. 8). Thus, MOND theories predict that in a merger, the gravity (or apparent dark matter) should mainly be located where the gas is located. In an advanced merger, the gas is located behind the galaxies.

The location of the gravity (or apparent dark matter) can be determined from weak gravitational lensing observations of the cluster [7, 30]. This test has been performed on the “Bullet Cluster” 1E0657-56 [7, 30], where the weak lensing measurement show that the gravity of the merging subcluster is centered on the galaxies, and is clearly displaced from the located of the sub-cluster gas. Thus, these measurements provide what is arguably the strongest proof of the existence of dark matter, rather than a change in the laws of gravity.

Another alternative to the conventional Cold Dark Matter hypothesis is that the dark matter consists of weakly interacting elementary particles, but the particles do have a small but significant cross-section for self-interaction [42]. If this were the case, the dark matter would act as a collisional fluid, and would be displaced from the position of the galaxies in a merging cluster towards the center of the subcluster gas. In the “Bullet Cluster” 1E0657-56 no such displacement is evident [30], and the lack of such a displacement can be used to set an upper limit on the self-interaction cross-section per unit mass of dark matter of  $< 1 \text{ cm}^2 \text{ g}^{-1}$ . This is a very serious constraint on models of self-interacting dark matter.

## 12 Mergers and Cool Cluster Cores

### 12.1 Cooling Flows vs. Mergers

The centers of a significant fraction of clusters of galaxies have luminous cusps in their X-ray surface brightness known as “cooling flows” (see [12] for an extensive review). In every case, there is a bright (cD) galaxy at the center of the cooling flow region. The intracluster gas densities in these regions are much higher than the average values in the outer portions of clusters. X-ray spectra indicate that there are large amounts of gas at low temperatures (down to  $\sim 10^7 \text{ K}$ ), which are much cooler than those in the outer parts of clusters. The high densities imply rather short cooling times  $t_{\text{cool}}$  (the time scale for the gas to cool to low temperature due to its own radiation). The hypothesis is that the gas in these regions is cooling from higher intracluster temperature ( $\sim 10^8 \text{ K}$ ) down to these lower temperatures as a result of the energy loss due to the X-ray emission we observe. Typical cooling rates are  $\sim 100 M_{\odot} \text{ yr}^{-1}$ . The cooling times, although much shorter than the Hubble

time, are generally much longer than the dynamical (i.e., sound crossing time) of the gas in these regions. As a result, the gas is believed to remain nearly in hydrostatic equilibrium. Thus, the gas must compress as it cools to maintain a pressure which can support the weight of the overlying intracluster medium.

The primary observational characteristics of cooling flows are very bright X-ray surface brightnesses which increase rapidly toward the center of the cluster. The high surface brightnesses imply high gas densities which also increase rapidly towards the cluster center. These regions contain cooler cluster gas.

Empirically, there is significant indirect evidence that mergers disrupt cooling flows. There is a strong statistical anticorrelation between cooling flows and/or cooling rates, and irregular structures in clusters as derived by statistical analysis of their X-ray images [3]. Looked at individually, very strong cooling cores are almost never associated with very irregular or bimodal clusters, which are likely merger candidates [9, 17]. There are some cases of moderate cooling flows in merging clusters; in most cases, these appear to be early-stage mergers where the merger shocks haven't yet reached the cooling core of the cluster. Examples may include Cygnus-A [26] and Abell 85 [19]. There also are a large number of merging clusters at a more advanced stage with relatively small cooling cores; Abell 2065 [26] may be an example. Recently, Chandra Observatory X-ray images have shown a number of merging clusters with rapidly moving cores of cool gas (the "cold fronts" discussed below in Sect. 12.2). In these systems, the cooling flows appear to have survived, at least to the present epoch in the merger.

It is unclear exactly how and under what circumstances mergers disrupt cooling flows. The cooling flows might be disrupted by tidal effects, by shock heating the cooler gas, by removing it dynamically from the center of the cluster due to ram pressure, by mixing it with hotter intracluster gas, or by some other mechanism. Numerical hydrodynamical simulations are needed to study the mechanisms by which cooling flows are disrupted. This is a relatively unexplored area, largely because the small spatial scales and rapid cooling time scales in the inner regions of cooling flows are still a significant challenge to the numerical resolution of hydrodynamical codes. McGlynn and Fabian [32] argued that mergers disrupted cooling flows, but this was based on purely N-body simulations. Hydrodynamical simulations have been made of the effects of head-on mergers with relatively small subclusters ( $1/4$  or  $1/16$  of the mass of the main cluster) on a cooling flow in the main cluster [16]. They find that the mergers disrupt the cooling flow in some cases, but not in others. Their simulations suggest that the disruption is not due to tidal or other gravitational effects.

Another possibility is that the merger shocks heat up the cooling flow gas and stop the cooling flow. In the simulations, this does not appear to be the main mechanism of cooling flow disruption. There are a number of simple arguments which suggest that merger shocks should be relatively inefficient at disrupting cooling flows. First, it is difficult for these shocks to penetrate the high densities and steep density gradients associated with cooling flows,

and the merger shocks would be expected to weaken as they climb these steep density gradients. Even without this weakening, merger shocks have low Mach numbers, and only produce rather modest increases in temperature ( $\lesssim$  a factor of 2). These small temperature increases are accompanied by significant compressions. As a result, shock heating actually decreases the cooling time due to thermal bremsstrahlung emission for shocks with Mach numbers  $\mathcal{M} \leq (21 + 12\sqrt{3})^{1/2} \approx 6.5$ . It is likely that the shocked gas will eventually expand, and adiabatic expansion will lengthen the cooling time. However, even if the gas expands to its preshock pressure, the increase in the cooling time is not very large. For a  $\mathcal{M} = 2$  shock, the final cooling time after adiabatic expansion to the original pressure is only about 18% longer than the initial cooling time.

The simulations by [16] suggest that the main mechanism for disrupting cooling flows is associated with the ram pressure of gas from the merging subcluster. The gas in the cooling flow is displaced, and may eventually mix with the hotter gas [39]. Earlier, [13] had argued that ram pressure, rather than shock heating, was the main mechanism for disrupting cooling flows. Assuming this is the case, one expects that the merger will remove the cooling flow gas at radii which satisfy

$$\rho_{\text{sc}} v_{\text{rel}}^2 \gtrsim P_{\text{CF}}(r), \quad (51)$$

where  $P_{\text{CF}}(r)$  is the pressure profile in the cooling flow,  $\rho_{\text{sc}}$  is the density of the merging subcluster gas at the location of the cooling flow, and  $v_{\text{rel}}$  is the relative velocity of the merging subcluster gas and the cooling flow. Reference [16] finds that this relation provides a reasonable approximation to the disruption in their simulations.

The pressure profile in the cooling flow gas prior to the merger is determined by the condition of hydrostatic equilibrium. If the cluster gravitational potential has a wide core within which the potential is nearly constant (e.g., as in a King model), then the cooling flow pressure will not increase rapidly into the center. In this case, once the merger reaches the central regions of the cluster, if the ram pressure is sufficient to remove the outer parts of the cooling flow, it should be sufficient to remove nearly all of the cooling flow. On the other hand, if the cluster potential is sharply peaked as is predicted by numerical simulations [35], the merger may remove the outer parts of the cooling flow but not the innermost regions. Thus, the survival and size of cool cores in merging clusters can provide evidence on whether clusters have sharply peaked potentials [26].

## 12.2 Cold Fronts

One of the more dramatic early discoveries with the Chandra X-ray Observatory was the presence of very sharp surface brightness discontinuities in merging clusters of galaxies. A pair of such discontinuities were first seen in

the public science verification data on the Abell 2142 cluster [28]. Initially, it seemed likely that these were merger shocks. However, temperature measurements showed that this was not the case. The high X-ray surface brightness regions were both dense and *cool*; thus, the gas in these regions had a lower specific entropy than the gas in the less dense regions. The lack of a pressure jump and the incorrect sign of the temperature and entropy variations showed that these features could not be shocks [28]. Instead, they appear to be contact discontinuities between hot, diffuse gas and a cloud of colder, denser gas [28]. In [47], these contact discontinuities were named “cold fronts.” Reference [28] argues that the source of the cold clouds are the cooling cores of one or both of merging subclusters. As noted above, cooling flows do appear to be able to partially survive in mergers, at least for some period. Subsequently, cold fronts have been observed in a number of other clusters; for an extensive review of the observations of these cold fronts, see [14].

### Kinematics of Cold Fronts

As discussed extensively in [47], the variation in the density, pressure, and temperature of the gas in a cold front can be used to determine the relative velocity of cold core. This technique is analogous to that for merger shocks discussed above (47) and (48). The geometry is illustrated in Fig. 2, which is drawn in the rest frame of the cold core. We assume that the cold core has a smoothly curved, blunt front edge. The normal component of the flow of hot gas past the surface of the cold core will be zero. There will be at least one point where the flow is perpendicular to the surface of the cold core, and the flow velocity of the hot gas will be zero at this stagnation point (“st” in Fig. 2). Far upstream, the flow of the hot gas will be undisturbed at the velocity of the cold core relative to the hotter gas,  $v_1$ . Let  $c_{s1}$  be the sound speed in this upstream gas, and  $\mathcal{M}_1 \equiv v_1/c_{s1}$  be the Mach number of the motion of the cold core into the upstream gas. If  $\mathcal{M}_1 > 1$ , a bow shock will be located ahead of the cold front.

The ratio of the pressure at the stagnation point to that far upstream is given by [20]

$$\frac{P_{\text{st}}}{P_1} = \begin{cases} (1 + \frac{\gamma-1}{2}\mathcal{M}_1^2)^{\frac{\gamma}{\gamma-1}}, & \mathcal{M}_1 \leq 1 \\ \mathcal{M}_1^2 (\frac{\gamma+1}{2})^{\frac{\gamma+1}{\gamma-1}} \left(\gamma - \frac{\gamma-1}{2\mathcal{M}_1^2}\right)^{-\frac{1}{\gamma-1}}, & \mathcal{M}_1 > 1. \end{cases} \quad (52)$$

The ratio ( $P_{\text{st}}/P_1$ ) increases continuously and monotonically with  $\mathcal{M}_1$ . Thus, in principle, measurements of  $P_1$  and  $P_{\text{st}}$  in the hot gas could be used to determine  $\mathcal{M}_1$ . The pressures would be determined from X-ray spectra and images. In practice, the emissivity of the hot gas near the stagnation point is likely to be small. However, the pressure is continuous across the cold front, so the stagnation pressure can be determined just inside of the cold core, where the X-ray emissivity is likely to be much higher. Once  $\mathcal{M}_1$  has been determined, the velocity of the encounter is given by  $v_1 = \mathcal{M}_1 c_{s1}$ .

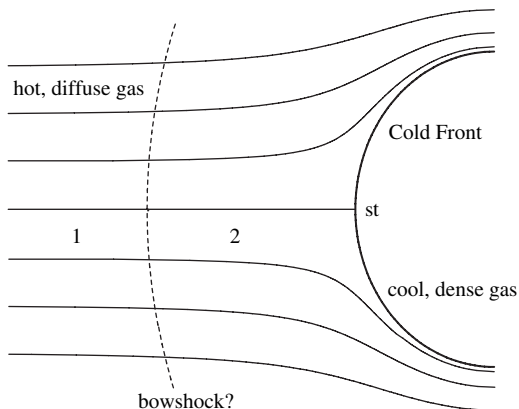


**Fig. 2.** A schematic diagram of flow around a “cold front” in a cluster merger. The heavy solid arc at the right represents the contact discontinuity between the cold, dense cold core gas, and the hotter, more diffuse gas from the outer regions of the other cluster. The cold core is moving toward the left relative to the hotter gas. The narrow solid lines are streamlines of the flow of the hotter gas around the cold core. The region labelled “1” represent the upstream, undisturbed hot gas. If the cold front is moving transonically ( $\mathcal{M}_1 > 1$ ), then the cold front will be preceded by a bow shock, which is shown as a dashed arc. The stagnation point, where the relative velocity of the cooler dense gas and hotter diffuse gas is zero, is marked “st”

If the motion of the cold core is transonic ( $\mathcal{M}_1 > 1$ ), one can also determine the velocity from the temperature and/or density jump at the bow shock (47) and (48). If the bow shock can be traced to a large transverse distance and forms a cone, the opening angle of this Mach cone corresponds to the Mach angle,  $\theta_M \equiv \csc^{-1}(\mathcal{M}_1)$ . However, variations in the cluster gas temperature may lead to distortions in this shape.

The distance between the stagnation point and the closest point on the bow shock (the shock “stand-off” distance  $d_s$ ) can also be used to estimate the Mach number of the motion of the cold front [47]. The ratio of  $d_s$  to the radius of curvature of the cold front  $R_{cf}$  depends on the Mach number  $\mathcal{M}_1$  and on the shape of the cold front. Figure 3 shows the values of  $d_s/R_{cf}$  as a function of  $(\mathcal{M}_1^2 - 1)^{-1}$  for a spherical cold front [41]. Although there is no simple analytic expression for the stand-off distance which applies to all shapes of objects, a fairly general approximate method to calculate  $d_s$  has been given by [34], and some simple approximate expressions exist for a number of simple geometries. The stand-off distance increases as the Mach number approaches unity; thus, this method is, in some ways, a very sensitive diagnostic for the Mach number for the low values expected in cluster mergers. On the other hand, the stand-off distance also depends strongly on the shape of the cold front as the Mach number decreases. The application of this diagnostic to observed clusters is strongly affected by projection effects. Because the radius

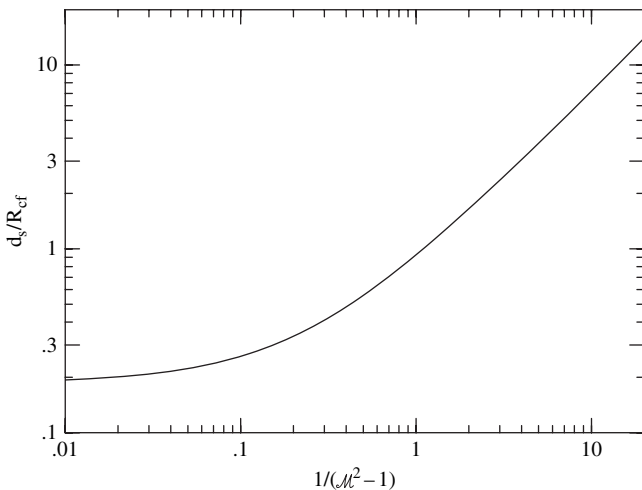


**Fig. 3.** The ratio of the stand-off distance of the bow shock  $d_s$  to the radius of curvature  $R_{cf}$  of the stagnation region of the cold front, as a function of  $1/(\mathcal{M}_1^2 - 1)$ , where  $\mathcal{M}_1$  is the Mach number. This is for a spherical cold front and  $\gamma = 5/3$

of curvature of the bow shock is usually greater than that of the cold front, projection effects will generally cause  $d_s$  to be overestimated and  $\mathcal{M}_1$  to be underestimated. Projection effects also make the true shape of the cold front uncertain.

These techniques have been used to determine the merger velocities from cold fronts in Abell 3667 [47], RXJ1720.1+2638 [31], and Abell 85 [19]. The most spectacular application is the “Bullet Cluster” 1E0657-56 [7, 29, 30], which contains a very high Mach number merger.

### Width of Cold Fronts

One remarkable aspect of the cold fronts observed with the Chandra Observatory in several clusters is their sharpness. In Abell 3667, the temperature changes by about a factor of two across the cold front [47], and the accompanying change in the X-ray surface brightness occurs in a region which is narrower than 2 kpc [47]. This is less than the mean-free-path of electrons in this region. The existence of this very steep temperature gradient and similar results in other merging clusters with cold fronts requires that thermal conduction be suppressed by a large factor [11, 46, 47] relative to the classical value in an unmagnetized plasma (14) [43]. It is likely that this suppression is due to the effects of the intracluster magnetic field. It is uncertain at this point whether this is due to a generally tangled magnetic field (in which case, heat conduction might be suppressed throughout clusters), or due to a tangential magnetic field specific to the tangential flow at the cold front [46].

Because of the tangential shear flow at the cold front (Fig. 2), the front should be disturbed and broadened by the Kelvin–Helmholtz (K–H) instability. Reference [46] argues that the instability is suppressed by a tangential magnetic field, which is itself generated by the tangential flow. This suppression requires that the magnetic pressure  $P_B$  be a non-trivial fraction of the gas pressure  $P$  in this regions,  $P_B \gtrsim 0.1P$ . The required magnetic field strength in Abell 3667 is  $B \sim 10 \mu\text{G}$ . Alternatively, cold fronts might be stabilized by gravity [15] or acceleration along the front [6].

## References

1. Allen, S.W., Schmidt, R.W., Ebeling, H., Fabian, A.C., van Speybroeck, L.: MNRAS **353**, 457 (2004)
2. Bennett, C.L., et al.: ApJS **148**, 1 (2003)
3. Buote, D.A., Tsai, J.C.: ApJ **458**, 27 (1996)
4. Cavaliere, A., Fusco-Femiano, R.: A&A **49**, 137 (1976)
5. Cavaliere, A., Lapi, A., Menci, N.: ApJ **581**, L1 (2002)
6. Churazov, E.: Physics of cluster cores. In: The X-ray Universe 2005, (in press)
7. Clowe, D., Gonzalez, A., Markevitch, M., et al.: ApJ **604**, 596 (2004)
8. Davé, R.: ApJ **552**, 473 (2001)
9. Edge, A.C., Stewart, G.C., Fabian, A.C.: MNRAS **258**, 177 (1992)
10. Eke, V.R., Navarro, J.F., Frenk, C.S.: ApJ **503**, 569 (1998)
11. Ettori, S., Fabian, A.C.: MNRAS **317**, L57 (2000)
12. Fabian, A.C.: ARA&A **32**, 277 (1994)
13. Fabian, A.C., Daines, S.J.: MNRAS **252**, 17p (1991)
14. Forman, W., Jones, C., Markevitch, M., Vikhlinin, A., Churazov, E.: High angular resolution cluster observations with Chandra: a new view. In: Merging Processes in Galaxy Clusters, pp. 109–132. Kluwer, Dordrecht (2002)
15. Fujita, Y., et al.: ApJ **575**, 764 (2002)
16. Gómez, P.L., Loken, C., Roettiger, K., Burns, J.O.: ApJ **569**, 122 (2002)
17. Henriksen, M.J.: ApJ **407**, L13 (1988)
18. Kaiser, N.: MNRAS **222**, 323 (1986)
19. Kempner, J., Sarazin, C.L., Ricker, P.R.: ApJ **579**, 236 (2002)
20. Landau, L.D., Lifshitz, E.M.: Fluid Mechanics, Pergamon, Oxford (1959)
21. Loewenstein, M.: ApJ **532**, 17 (2000)
22. Lloyd-Davies, E.J., Ponman, T.J., Cannon, D.B.: MNRAS **315**, 689 (2000)
23. Markevitch, M.: ApJ **504**, 27 (1998)
24. Markevitch, M., Forman, W.R., Sarazin, C.L., Vikhlinin, A.: ApJ **503**, 77 (1998)
25. Markevitch, M., Govoni, F., Brunetti, G., Jerius, D.: ApJ **627**, 733 (2005)
26. Markevitch, M., Sarazin, C.L., Vikhlinin, A.: ApJ **521**, 526 (1996)
27. Markevitch, M., Vikhlinin, A.: ApJ **563**, 95 (2001)
28. Markevitch, M., et al.: ApJ **541**, 542 (2000)
29. Markevitch, M., et al.: ApJ **567**, L27 (2002)
30. Markevitch, M., et al.: ApJ **606**, 542 (2004)
31. Mazzotta, P., Markevitch, M., Vikhlinin, A., Forman, W.R., David, L.P., Van Speybroeck, L.: ApJ **555**, 205 (2001)

32. McGlynn, T.A., Fabian, A.C.: MNRAS **208**, 709 (1984)
33. Milgrom, M.: ApJ **270**, 365 (1983)
34. Moekel, W.E.: Approximate Method for Predicting Forms and Location of Detached Shock Waves Ahead of Plane or Axially Symmetric Bodies, NACA Technical Note 1921 (1949)
35. Navarro, J.F., Frenk, C.S., White, S.D.M.: ApJ **490**, 493 (1997)
36. Osterbrock, D.E.: Astrophysics of Gaseous Nebulae and Active Galactic Nuclei, pp. 53–65. University Science, Mill Valley (1989)
37. Ponman, T.J., Cannon, D.B., Navarro, J.F.: Nature **397**, 135 (1999)
38. Ponman, T.J., Sanderson, A.J., Finoguenov, A.: MNRAS **343**, 331 (2003)
39. Ricker, P.M., Sarazin, C.L.: ApJ **561**, 621 (2001)
40. Sarazin, C.L.: X-ray Emission from Clusters of Galaxies, Cambridge University Press, Cambridge (1988)
41. Schreier, S.: Compressible Flow, pp. 182–189. Wiley, New York (1982)
42. Spergel, D.N., Steinhardt, P.J.: Phys. Rev. Lett. **84**, 3760 (2000)
43. Spitzer Jr., L.: Physics of Fully Ionized Gases, Interscience, New York (1956)
44. Takizawa, M.: ApJ **520**, 514 (1999)
45. Takizawa, M.: ApJ **532**, 182 (2000)
46. Vikhlinin, A., Markevitch, M., Murray, S.M.: ApJ **549**, L47 (2001a)
47. Vikhlinin, A., Markevitch, M., Murray, S.M.: ApJ **551**, 160 (2001b)
48. Vikhlinin, A., Markevitch, M., Murray, S.S., Jones, C., Forman, W., Van Speybroeck, L.: ApJ **628**, 655 (2005)
49. Voevodkin, A., Vikhlinin, A.: ApJ **601**, 610 (2004)
50. Voit, G.M.: RMP **77**, 207 (2005)
51. Voit, G.M., Bryan, G.L.: Nature **414**, 425 (2001)
52. White, S.D.M., Frenk, C.S.: ApJ **379**, 52 (1991)
53. Wise, M.W., Sarazin, C.L.: ApJ, **415**, 58 (1993)